

Molecular Imaging of Atherosclerotic Plaque with ^{64}Cu -Labeled Natriuretic Peptide and PET

Yongjian Liu¹, Dana Abendschein², Geoffrey E. Woodard³, Raffaella Rossin¹, Kyle McCommis¹, Jie Zheng¹, Michael J. Welch¹, and Pamela K. Woodard¹

¹Department of Radiology, Washington University School of Medicine, St. Louis, Missouri; ²Department of Internal Medicine, Washington University School of Medicine, St. Louis, Missouri; and ³National Institute of Allergy and Infectious Diseases, Bethesda, Maryland

Cardiovascular disease is the leading cause of death worldwide. PET has the potential to provide information on the biology and metabolism of atherosclerotic plaques. Natriuretic peptides (NPs) have potent antiproliferative and antimigratory effects on vascular smooth-muscle cells (VSMCs) and, in atherosclerosis, participate in vascular remodeling, in which the expression of NP clearance receptors (NPR-Cs) is upregulated both in endothelium and in VSMCs. **Methods:** We investigated the potential of a C-type atrial natriuretic factor (C-ANF) to image developing plaque-like lesions *in vivo*. C-ANF was functionalized with 1,4,7,10-tetraazacyclododecane-1,4,7,10-tetraacetic acid (DOTA) and labeled with ^{64}Cu for noninvasive PET in a hypercholesterolemic rabbit with atherosclerotic-like lesions induced by air desiccation of a femoral artery, followed by balloon overstretch of the developing neointima. Histopathology and immunohistochemistry were performed to assess plaque development and NPR-C localization. **Results:** ^{64}Cu -DOTA-C-ANF uptake in the atherosclerotic region was visible on small-animal PET images, with the highest target-to-background ratio (3.59 ± 0.94) observed after the air desiccation-induced injury. Immunohistochemistry and immunofluorescence staining showed NPR-C near the luminal surface of the plaque and in VSMCs. PET and immunohistochemistry competitive blocking studies confirmed receptor-mediated tracer uptake in the plaque. With blocking, PET tracer localization of atherosclerotic to control arteries was decreased from 1.42 ± 0.02 to 1.06 ± 0.06 ($P < 0.001$). **Conclusion:** We demonstrated that ^{64}Cu -DOTA-C-ANF is a promising candidate tracer for *in vivo* PET of NPR-Cs on atherosclerotic plaques.

Key Words: atherosclerosis; PET; natriuretic peptide; vascular targeting

J Nucl Med 2010; 51:85–91

DOI: 10.2967/jnumed.109.066977

Cardiovascular disease is the leading cause of death worldwide, despite primary and secondary prevention (1). Each year, it affects an estimated 80 million people in the United States, causing a sudden cardiac event (acute coronary syndrome or sudden cardiac death) in more than 1 million people.

Atherosclerosis is a chronic, progressive disease with a long asymptomatic phase. Currently, most diagnostic modalities for atherosclerosis imaging are not able to provide information on the biology and metabolism of the plaque that may identify the stage of the disease (2–4). To date, of the nuclear imaging approaches available, PET has been widely evaluated for atherosclerosis imaging because of its superior sensitivity (3). Among the approaches, ^{18}F -FDG is the most investigated tracer but lacks the ability to specifically target atherosclerosis (5). The biology of atherosclerosis, however, provides several potential biomarkers for plaque imaging such as matrix metalloproteinases, annexin V, and angiogenesis integrins (6,7).

Natriuretic peptides (NPs) belong to another group of markers that appear to show promise for atherosclerotic plaque detection because they play an important role in protecting the cardiovascular system from the effect of volume overload (8). Although present throughout vascular smooth-muscle cells (VSMCs) and endothelium, NP receptors (NPRs) have been largely overlooked as a potential target for atherosclerosis imaging and treatment agents. Among the 3 members of the NP family, the C-type NP (CNP) directly affects immune cell recruitment *in vivo* and is a potent inhibitor of VSMC migration and proliferation (9). The NPs exert their antithrombotic effects by interacting with specific cell-surface NPRs (10). Of the 3 existing NPRs, the NP clearance receptor (NPR-C), representing approximately 95% of the 3-NPR population, is expressed during the growth and remodeling of VSMCs (11). Additionally, it is the only NPR that recognizes all the NPs and NP fragments containing as few as 5 conserved amino acids (Arg-Ile-Asp-Arg-Ile) (10). In humans, the expression of the NPR-C is upregulated in

Received Jun. 8, 2009; revision accepted Oct. 7, 2009.

For correspondence and reprints contact: Pamela K. Woodard, Department of Radiology, Washington University School of Medicine, 510 S. Kingshighway Blvd., Campus Box 8131, St. Louis, MO 63110.

E-mail: woodardp@mir.wustl.edu

COPYRIGHT © 2010 by the Society of Nuclear Medicine, Inc.

atherosclerotic plaques (12,13). Thus, several animal models have been established that mimic human atherosclerosis, and high levels of CNP and NPR-C in the neointima of the atherosclerotic-like plaques have been demonstrated (14,15).

In this study, we investigated the potential of a CNP fragment, the C-type atrial natriuretic factor (C-ANF) (11,16), to longitudinally image the progression of atherosclerosis in a rabbit model with PET by conjugating the C-ANF with 1,4,7,10-tetraazacyclododecane-1,4,7,10-tetraacetic acid (DOTA) and labeling it with ^{64}Cu (17).

MATERIALS AND METHODS

Synthesis of DOTA-C-ANF

C-ANF (rat ANF(4–23), Des-Gln¹⁸,des-Ser¹⁹,des-Gly^{20,22},des-Leu²¹) (Bachem) and DOTA-*N*-hydroxysuccinimide ester (DOTA-NHS) (Macrocylics) conjugation and purification were performed following standard procedures (18). The DOTA-conjugated C-ANF was purified by solid-phase extraction (C-18 Sep-Pak cartridges; Waters) and reversed-phase high-performance liquid chromatography (RP-HPLC), respectively. RP-HPLC was performed on a system equipped with a UV/VIS detector (Dionex) and a radioisotope detector (B-FC-3200; BioScan Inc.) on a C-18 analytic column (5 μm , 4.6 \times 220 mm; Perkin Elmer). The linear gradient was from 100% H₂O to 65% acetonitrile in 45 min at a flow rate of 1 mL/min and an ultraviolet absorbance at 210 nm. The conjugation efficiency was more than 95%, as determined by RP-HPLC. The presence of 1 DOTA per peptide was confirmed by liquid chromatography–electrospray ionization mass spectrometry on a 2695 separation and Micromass ZQ module (Waters).

^{64}Cu Labeling of DOTA-C-ANF

^{64}Cu (half-life = 12.7 h, β^+ = 17%, β^- = 40%) was produced on the Washington University Medical School CS-15 cyclotron by the ^{64}Ni (p,n) ^{64}Cu nuclear reaction at a specific activity of 0.74–2.96 GBq/ μg at the end of bombardment (19). DOTA-C-ANF (10 μg , \sim 5 nmol) was labeled with ^{64}Cu (0.37 GBq) in 200 μL of 0.1 M ammonium acetate buffer (pH 5.5) at 43°C for 1 h, with a yield of 78.5% \pm 4.8% (n = 23). The ^{64}Cu -DOTA-C-ANF conjugate was purified by solid-phase extraction, and the specific activity was 58.1 \pm 3.6 MBq/nmol. The identity of ^{64}Cu -DOTA-C-ANF was confirmed by liquid chromatography–mass spectrometry after decay (19).

Serum Stability of ^{64}Cu -DOTA-C-ANF

The stability of ^{64}Cu -DOTA-C-ANF was evaluated in rabbit serum (Sigma-Aldrich) at 37°C for 1 h and determined from the percentage of intact ^{64}Cu -DOTA-C-ANF in the radiochromatogram.

Tracer Blood Clearance Study

The pharmacokinetics of the tracer were determined in normal rabbits (n = 4). Approximately 20 MBq of ^{64}Cu -DOTA-C-ANF were injected intravenously into 1 ear of the rabbit, and blood samples (0.2 mL) were drawn from the contralateral ear at intervals of 1, 3, 5, 10, 20, 40, and 60 min. The activity of the blood samples was counted in a γ -counter (Beckman 8000) and expressed as a percentage injected dose per gram (%ID/g; n = 4).

Animal Preparations to Induce Atherosclerotic-like Lesions

All animal studies were performed in compliance with guidelines set forth by the National Institutes of Health Office of

Laboratory Animal Welfare and approved by the Washington University Animal Studies Committee. Atherosclerotic-like arterial lesions were induced in the right femoral artery of rabbits by air desiccation, followed by angioplasty at a later time point (TP), as reported previously (20). Briefly, male New Zealand White rabbits were fed a 0.25% cholesterol-enriched diet throughout the study, and elevated serum cholesterol (>200 mg/dL) was confirmed at the time of vessel injury. The right femoral artery was exposed aseptically through a longitudinal skin incision, and lidocaine was applied topically to prevent spasm. A 1- to 2-cm segment of the vessel was isolated between air-tight ligatures, and small branches were ligated with suture. A 27-gauge needle was used to puncture the isolated segment proximally as a vent. A second 27-gauge needle was inserted distally into the segment, and nitrogen gas was passed through the vessel at a flow rate of 80 mL/min for 8 min to dry and cause sloughing of the endothelium. The segment was then flushed with saline, and the ligatures were released to restore blood flow, with gentle pressure applied to the puncture sites for a few minutes to maintain hemostasis. The skin incision was closed, and the animal was allowed to recover from anesthesia.

Four to 6 wk after the air desiccation–induced injury, the lesion site and extent of stenosis in the femoral artery were identified by an angiogram obtained using a 4-French guide catheter introduced through a carotid arterial cutdown and advanced to the distal aorta. Heparin (100 U/kg, intravenously) was given to prevent clot formation in the catheters. A 0.036-cm guidewire was then advanced across the lesion, and the guide catheter was removed. A 2.0–2.5 \times 20 mm coronary angioplasty balloon was advanced over the guidewire, and the site of stenosis was dilated with three 30-s balloon inflations of 6–8 atmospheres, with 1 min between inflations. After reinjuring the lesion site, patency of the femoral artery was confirmed by an angiogram through the angioplasty catheter before the catheter was removed. The carotid was ligated, the skin incision closed, and the animal was allowed to recover from anesthesia. The left femoral artery remained uninjured as a control.

Imaging Protocol

The experimental design is schematized in Figure 1. To determine tracer uptake, 9 rabbits (mean weight \pm SD, 4.2 \pm 0.5 kg) were imaged by MRI and small-animal PET 4–6 wk after the air desiccation–induced injury (TP 1), 6 rabbits coming from TP 1 were imaged by MRI and PET 3 wk after the balloon overstretching–induced injury (TP 2), and 4 rabbits coming from TP 2 were imaged by MRI and PET 4 wk after TP 2 (TP 3). For each PET study, about 131 \pm 33 MBq (n = 23) of purified ^{64}Cu -DOTA-C-ANF (about 2 nmol) were administered. The baseline tracer uptake was measured in 1 healthy rabbit (4.6 kg) on a normal rabbit chow diet. The level of cholesterol in plasma was analyzed in each rabbit before imaging sessions. Samples of injured and control arteries were taken at each TP for histology and immunohistochemistry.

Competitive Receptor Blocking Studies

Competitive receptor blocking studies were performed on 4 rabbits (4.2 \pm 0.4 kg). Three rabbits at TP 2 were imaged with MRI and PET for a preblocking study to confirm the presence of atherosclerotic lesions and tracer uptake. One week after the scan, PET studies were performed after the coinjection of ^{64}Cu -DOTA-C-ANF with unlabeled C-ANF peptide (1 mg, C-ANF: ^{64}Cu -DOTA-C-ANF = 100:1 molar ratio). An additional blocking study was performed in an additional rabbit with atherosclerotic lesion at TP 1.

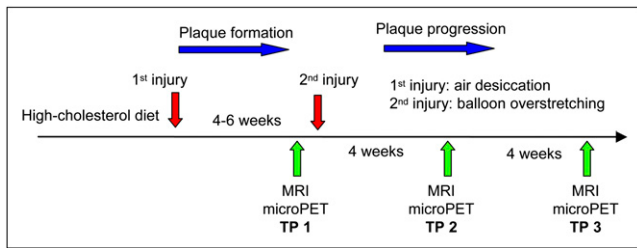


FIGURE 1. Schematic diagram of experimental design.

MRI Studies

The presence of atherosclerotic lesions in the rabbits was confirmed by 3-T MRI. T1-weighted (repetition time/echo time, 600 ms/12 ms; number of excitations, 10 min) turbo-spin-echo images were acquired 1 h after the intravenous administration of a non-receptor-specific plaque-targeting contrast agent (gado-fluorine M, 0.5 $\mu\text{mol/kg}$ of body weight; Bayer Schering Pharma AG) (17,21).

PET Studies

After the MRI scans, the rabbits were injected with ^{64}Cu -DOTA-C-ANF (144.3 ± 33.3 MBq), and 60-min dynamic scans were acquired on the microPET Focus-220 (Siemens Medical Solutions).

Data analysis of the small-animal PET images was performed using the manufacturer's software (ASI Pro). The accumulation of ^{64}Cu -DOTA-C-ANF at the injury site and on the contralateral, noninjured femoral artery (control) was calculated as standardized uptake values (SUVs) in 3-dimensional regions of interest by averaging the activity concentration corrected for decay over the contained voxels (multiple image slices) (22). SUVs were not corrected for partial-volume effects.

After the last PET scan, the animals were euthanized by exsanguination, and the femoral vessels were perfusion-fixed in situ with freshly prepared 4% paraformaldehyde solution. Tissue samples containing the injured and control arteries were harvested for histopathology and immunohistochemistry.

Histopathology

Vessel specimens were embedded in paraffin and step-sectioned (10 μm) transversely at 1-mm intervals to approximate the distance between MRI slices, and the sections were stained with hematoxylin and eosin and Verhoeff's Van Gieson stain for elastin. The sections were examined to identify the plaque components including foam cells and VSMCs.

Immunohistochemistry

Immunohistochemistry was performed on paraffin-embedded sections from both the injured and the noninjured control arteries of each rabbit. For immunohistochemistry, an anti-NPR-C antibody (Abgent; 1:100) was used, followed by a secondary fluorescein isothiocyanate-conjugated antirabbit antibody (Invitrogen; 1:1,000). The slides were viewed with a laser scanning microscope and the image browser (LSM510 META; Carl Zeiss). Blocking studies for NPR-C were performed by competitively blocking the primary antibody binding by preincubation of diluted antibody (NPR-C rabbit; Abgent) with the cognate peptide (0.5 mg/mL) overnight at 4°C before immunohistochemistry staining. The absence of a primary antibody was used as a negative control.

Additional immunofluorescent staining was performed for colocalization of NPR-C. Dual immunofluorescence staining was performed with vascular cell adhesion molecule-1 (VCAM-1) to identify NPR-C within the endothelium and with anti- α -smooth muscle actin (Sigma-Aldrich) to identify NPR-C within VSMCs. Fluorescein isothiocyanate, Rhodamine (Jackson Immunologicals), and Alexafluor 488, 568 (Invitrogen) were used for secondary antibody staining. This colocalization immunofluorescence was performed on femoral artery atherosclerotic specimens at all TPs and with a normal control artery.

Statistical Analysis

Results are expressed as mean and SD. The 2-tailed paired and unpaired Student *t* tests were used to test differences within animal groups (injured artery vs. control artery) and between groups of animals imaged at different TPs (such as TP 1 vs. TP 2), respectively. The significance level in all tests was *P* less than or equal to 0.05. GraphPad Prism, version 4.0 (GraphPad Software), was used for all statistical analyses.

RESULTS

^{64}Cu Labeling and Serum Stability of ^{64}Cu -DOTA-C-ANF

The radiochemical purity of the ^{64}Cu -DOTA-C-ANF was always higher than 98%, confirmed by radio-HPLC. The mass spectrometry of the decayed ^{64}Cu -DOTA-C-ANF showed 1 DOTA conjugated to 1 C-ANF peptide. The radio-HPLC analysis showed $97.7\% \pm 3.9\%$ ($n = 3$) intact ^{64}Cu -DOTA-C-ANF after a 1-h incubation at 37°C, indicating the stability of the tracer in rabbit serum.

Blood Clearance of ^{64}Cu -DOTA-C-ANF

The blood curve showed that at 1 min after injection the activity left in blood was 0.22 %ID/g, which decreased sharply to 0.10 %ID/g in 2 min and declined slowly to 0.02 %ID/g at 60 min after injection ($n = 4$) (Fig. 2).

Plasma Cholesterol Levels

At the time of imaging, the rabbits on a high-cholesterol diet had $1,111 \pm 366$ mg/dL, $1,451 \pm 421$ mg/dL, and $1,554 \pm 265$ mg/dL total plasma cholesterol at TP 1, TP 2, and TP 3, respectively (reported normal baseline value of total plasma cholesterol, 72 ± 12 mg/dL) (17).

Histopathology

Histology of femoral artery sections obtained at TP 1 confirmed the formation of primary neointimal lesions comprising VSMCs, foam cells, and extracellular matrix at the injury site (Fig. 3B). Specimens obtained at TPs 2 and 3 showed disruption of the internal elastic lamina and a luminal stenotic lesion that was largely acellular (Figs. 3C and 3D). No evidence of fibrous cap thinning, fissures, or thrombosis suggesting instability was observed. The sections obtained from the contralateral uninjured arteries showed no neointimal formation, despite the presence of high-cholesterol plasma (Fig. 3A).

Immunohistochemistry

Immunohistochemistry and staining performed for colocalization confirmed the presence of NPR-C primarily within the atherosclerotic plaque or neointima (Figs. 3 and

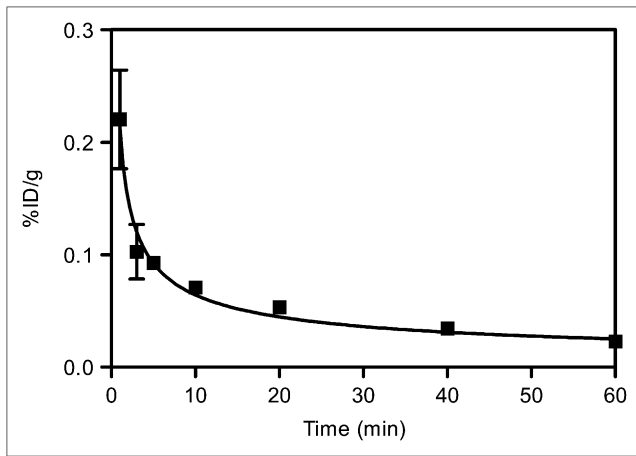


FIGURE 2. Blood clearance of ⁶⁴Cu-DOTA-C-ANF in rabbits.

4) but also at the vascular smooth-muscle-neointima interface. Staining was relatively increased in the injured arteries, compared with the noninjured control arteries. NPR-C presence also appeared to be the highest in specimens obtained at TP 1 (Figs. 3B and 4A), compared

with TP 2 (Figs. 3C and 4C) and TP 3 (Fig. 3D). Colocalization with VCAM-1 demonstrated little endothelium present within the lesion.

Separate competitive blocking studies demonstrated decreased immunostaining for NPR-C, further confirming the presence of the receptor (Figs. 3A and 3B).

MRI of Gadofluorine Uptake in Atherosclerotic-like Lesions

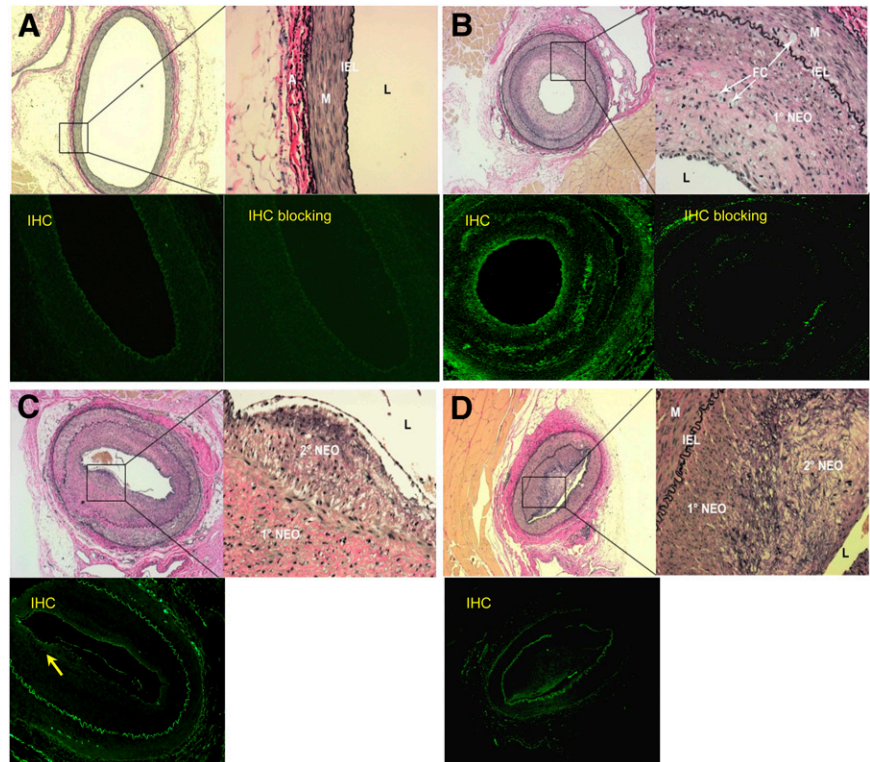
The injured vessels in all rabbits at all TPs demonstrated increased signal secondary to gadofluorine M uptake. The sites of injury visible on MRI also correlated with regions of increased radiotracer activity seen with PET. The control arteries showed no gadofluorine M uptake (Fig. 5).

Quantitative PET of ⁶⁴Cu-DOTA-C-ANF in Atherosclerotic-like Lesions

PET images clearly show the ⁶⁴Cu-DOTA-C-ANF tracer uptake at the site of induced atherosclerosis, with significant differences from noninjured control vessels in all animals.

Figure 6A shows a representative PET transverse slice from 1 rabbit injected with ⁶⁴Cu-DOTA-C-ANF (5- to 60-min summed frames). The tracer uptake in the injured site was clearly visualized by PET and stabilized over the 1-h

FIGURE 3. Light micrographs of femoral arterial cross-sections from hypercholesterolemic rabbits obtained at 3 TPs after injury and stained with Verhoeff's Van Gieson for elastin and fluorescent images of corresponding sections immunostained for NPR-C or blocked before immunostaining. Low-power micrographs are at $\times 4$ magnification, high-power insets are $\times 400$ magnification. L = lumen. (A) Control femoral artery from TP 2 rabbit shown in C. Inset shows intact internal elastic lamina (IEL), medium (M), and adventitia (A). Uninjured, control femoral artery shows only IEL autofluorescence. Control femoral artery immunofluorescence after competitive blocking of antibody-antigen binding shows no difference, compared with preblocked image. (B) Injured femoral artery at TP 1. Inset shows primary neointima (1° NEO) containing numerous foam cells (FCs) and dark nuclei of VSMC. Immunohistochemistry shows increased fluorescence near luminal or endothelial surface of primary neointima (arrow). TP 1 immunofluorescence after competitive blocking of antibody-antigen binding indicates specific binding of primary antibody to NPR-C. (C) Injured femoral artery at TP 2 showing broken IEL (adjacent to inset box) and development of amorphous, less cellular secondary neointima (2° NEO), shown in inset. Endothelium is artifactually lifted away from neointima. Immunohistochemistry shows some fluorescence on less cellular secondary neointima. (D) Injured femoral artery at TP 3 showing enlarged 2° NEO comprising predominantly matrix and elastin elements, with few cells. Immunohistochemistry shows some fluorescence on less cellular secondary neointima. In all immunostained images, IEL demonstrates autofluorescence. IHC = immunohistochemistry.



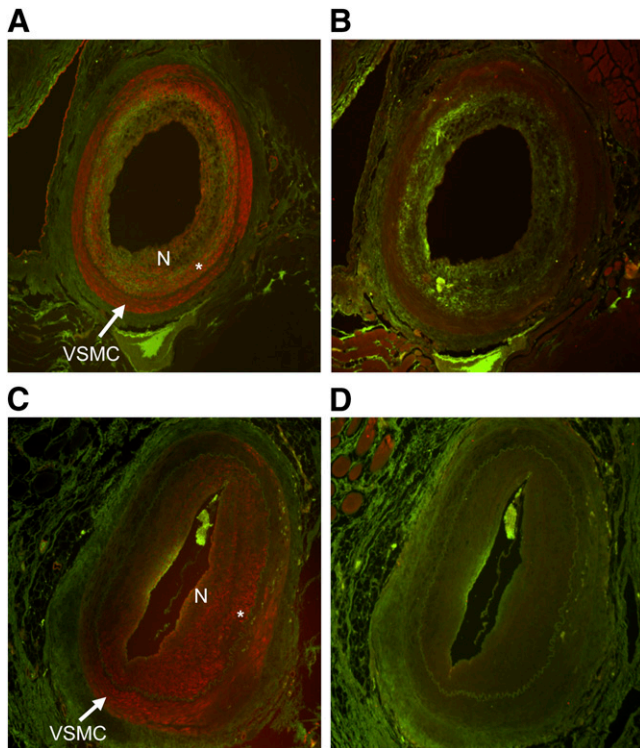


FIGURE 4. Micrographs of NPR-C colocalization with VSMC and endothelium at TP 1 and TP 2. (A) NPR-C (green) colocalized with VSMC (red) using anti- α -smooth muscle actin (SM) at TP 1. (B) NPR-C (green) colocalized with endothelium (red) using VCAM-1. (C) NPR-C colocalized with VSMC using SM at TP 2. (D) NPR-C colocalized with endothelium (red) using VCAM-1 at TP 2. N = neointimal proliferation. *VSMC–neointimal proliferation interface.

scan (Fig. 6C). The highest uptake at the injury site was observed at TP 1 (SUV, 2.01 ± 0.36) and decreased at later TPs (Fig. 7A). Noticeably, the uptake of ^{64}Cu -DOTA-C-ANF on the injured vessel was significantly higher than that on the control artery ($P < 0.05$) and muscle ($P < 0.005$) at each considered TP. The target-to-background (injured artery-to-muscle) SUV ratio reached the highest value at TP 1 (3.59 ± 0.94) (Fig. 7B). This value decreased significantly ($P < 0.05$) at TP 2 and remained constant at TP 3. On the contrary, no significant differences were observed in the control artery-to-muscle ratio at the 3 TPs.

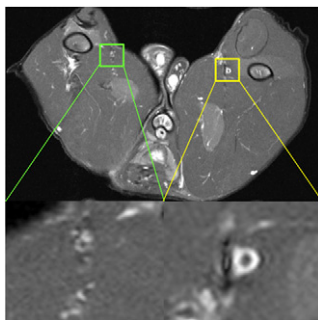


FIGURE 5. MR T1-weighted transverse image of typical atherosclerotic lesion in femoral artery of rabbit at TP 1.

The injured artery-to-muscle SUV ratio was significantly higher than that of control artery-to-muscle at each TP ($P < 0.05$). Additional PET images at 3 TPs are shown in Supplemental Figures 1–3 (supplemental materials are available online only at <http://jnm.snmjournals.org>).

Competitive receptor blocking performed in animals at TP 1 ($n = 1$) and TP 2 ($n = 3$) resulted in similar ^{64}Cu -DOTA-C-ANF uptakes and SUVs on both injured arteries and noninjured controls (Figs. 6B and 6D). In these experiments, the SUV ratio of injured to control arteries (TP 1, 1.08; TP 2, 1.07 ± 0.06) was significantly lower than that obtained in the preblocking studies (TP 1, 2.14; TP 2, 1.42 ± 0.03) ($P < 0.05$). Also, because of receptor blocking, the target-to-background ratio at TP 2 was reduced from 3.05 ± 0.19 to 2.13 ± 0.18 ($P < 0.01$). In contrast, the control artery-to-muscle ratio was not altered significantly (2.19 ± 0.16 vs. 2.00 ± 0.06 , $P > 0.05$).

DISCUSSION

In this study, we demonstrated the capability of a newly developed PET tracer to specifically image the status of the NPR-C expressed on atherosclerotic-like plaques by choosing the C-ANF fragment (16), functionalized with DOTA and labeled with ^{64}Cu .

In the rabbit model, the initial air-desiccation arterial injury combined with a cholesterol-enriched diet (TP 1) led to neointimal thickening, with lesions composed of many VSMCs and foam cells (Figs. 3B and 4A). Histopathologic images and VCAM-1 immunostaining obtained at TP 2 showed the development of increased neointimal thickening containing more cellular matrix and fewer VSMCs (Figs. 3C and 4C). At TP 3, the lumen is almost blocked because of the proliferation of neointimal tissue (Fig. 3D).

In this study, the rabbits were imaged by MRI to confirm the presence of lesions at the injury site before PET. It has been reported that gadofluorine M accumulates within the fibrous plaque or in the fibrous cap of a plaque containing a high amount of extracellular matrix components through nonspecific hydrophobic interactions with the plaque material (21). As shown in Figure 5, gadofluorine M accumulated significantly on the injured femoral artery, producing high contrast in comparison to the surrounding tissue whereas little uptake was observed on the noninjured control artery.

Removal of the arterial endothelium by air desiccation has been shown to result in the recruitment of VSMCs and proliferation of the neointima (20). As a response, CNP is synthesized by smooth muscle cells to inhibit the growth, which activates the expression of NPR-C on the cells concurrently (12,14). At TP 2 and TP 3, the decreased cellular content of the neointimal tissue correlated with the decrease of the NPR-C (23). Our PET scan showed a high accumulation of ^{64}Cu -DOTA-C-ANF at the lesion site (Fig. 6A). At TP 1, both the SUV and the target-to-background ratio reached the maximum among the 3 TPs (Figs. 7A and

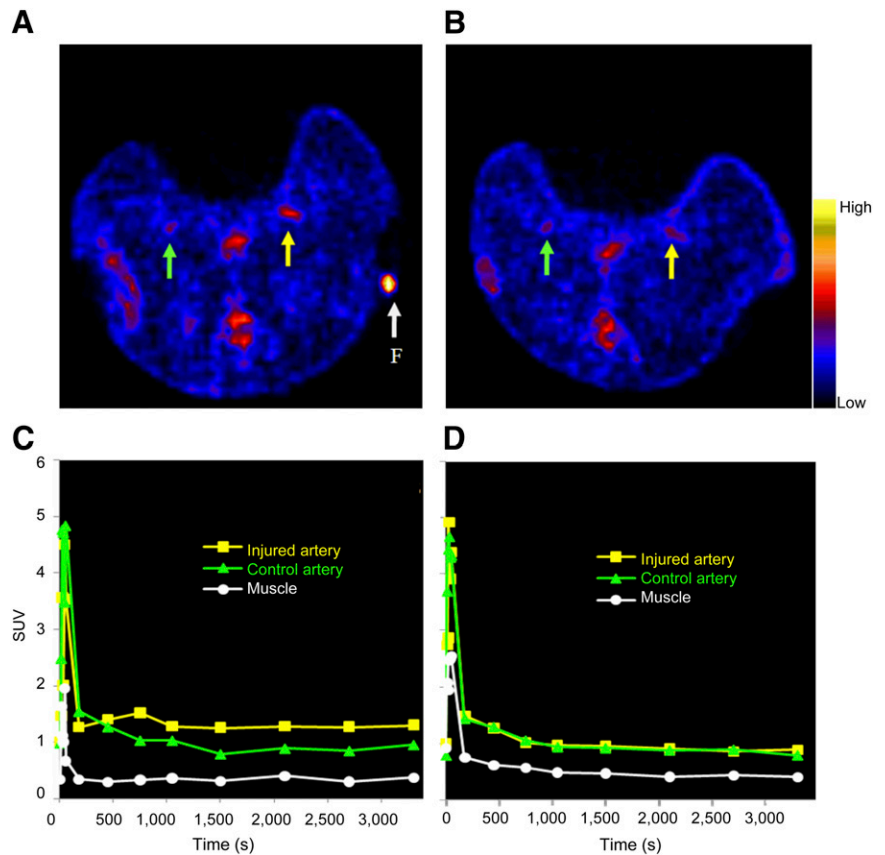


FIGURE 6. Uptake of ^{64}Cu -DOTA-C-ANF on injured (yellow arrow and curve) and control (green arrow and curve) arteries in rabbits from TP 1. (A) Representative transverse PET slice, preblocking study. (B) Representative transverse PET slice, blocking study. (C) Time-activity curves of image in A. (D) Time-activity curves of image in B. F (arrow) = fiducial marker.

7B), reasonably because of the high expression of the NPR-C on the proliferating VSMC. With the progression of the plaque and increase in acellular tissue, the VSMC population and expression of NPR-C receptor on the lesion decreased (Figs. 3C, 3D, and 4C). This decrease was mirrored by a decrease in tracer uptake (Figs. 7A and 7B). Our results suggest that ^{64}Cu -DOTA-C-ANF will likely be of utility in assessing the development of atherosclerosis early and at neointimal injury but of less utility as an atherosclerotic plaque progresses and becomes relatively acellular.

Besides immunohistochemistry, the NPR-C-mediated accumulation of ^{64}Cu -DOTA-C-ANF in atherosclerotic lesions was also confirmed by PET in competitive receptor blocking studies at TP 1 and TP 2. The coadministration of excess C-ANF decreased the tracer uptake in the lesion site to a level similar to that of the control artery (Figs. 6B and 6D). The target-to-background ratio was also significantly lower than that observed in preblocking experiments. A similar decrease in receptor expression was observed in immunohistochemistry experiments *ex vivo* (Figs. 3A and 3B).

In atherosclerosis PET, the slow clearance of tracer from the blood may decrease the sensitivity and cause ambiguous results (24–26). However, ^{64}Cu -DOTA-C-ANF cleared from the blood within a few minutes (Fig. 2). This explains the sharp decrease of radioactivity, followed by a plateau

observed at both injury and control sites during PET scans (Figs. 6C and 5D). The SUVs obtained with ^{64}Cu -DOTA-C-ANF in atherosclerotic lesions are higher than those obtained with the other reported tracers, such as ^{18}F -FDG and ^{111}In -LDL (27,28), and comparable to those obtained with $^{99\text{m}}\text{Tc}$ -annexin-V (29). Candidate tracers such as ^{125}I -monocyte chemoattractant peptide 1 and $^{99\text{m}}\text{Tc}$ -labeled anti-lectin-like oxidized low-density lipoprotein receptor-1 antibody exhibited a higher accumulation in atherosclerotic plaques (30,31). Because of the specific activity of ^{64}Cu -DOTA-C-ANF (58.1 ± 3.6 MBq/nmol), the SUVs reported here were obtained by injecting 1.1 ± 0.3 μg of C-ANF per kilogram of body weight. We expect a markedly improved sensitivity if the targeting peptide is conjugated to a nanostructure carrying multiple copies of ^{64}Cu -DOTA.

CONCLUSION

In this study, we demonstrated that the presence of the NPR-C in atherosclerotic plaque can be imaged noninvasively with ^{64}Cu -DOTA-C-ANF and PET. The developed tracer met the criteria of a modern molecular imaging probe for *in vivo* atherosclerotic plaque imaging because of the high sensitivity, specificity, and fast blood clearance. Further assessment in additional animal models and *ex vivo* human specimens will be necessary to demonstrate the full potential of this radiotracer in the assessment of atherosclerotic plaque.

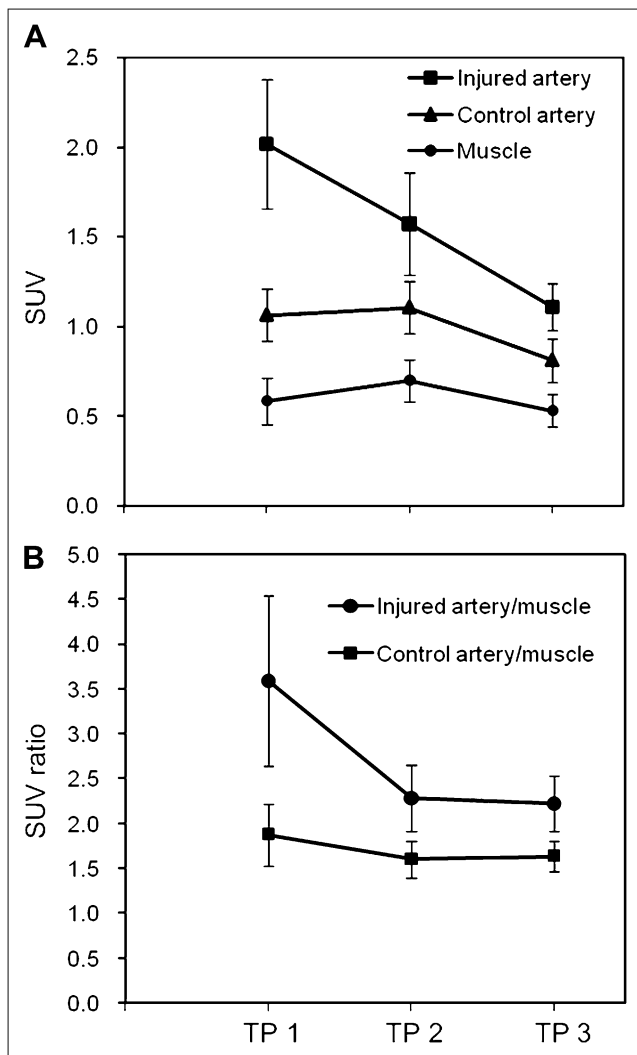


FIGURE 7. (A) ^{64}Cu -DOTA-C-ANF tracer uptake SUV on injured femoral arteries, noninjured control arteries, and surrounding muscle at 3 experimental TPs, representing progression and remodeling of atherosclerotic plaques. (B) SUV ratios of tracer uptake at each TP (TP 1, $n = 9$; TP 2, $n = 6$; and TP 3, $n = 4$).

ACKNOWLEDGMENTS

We thank Terry Sharp, Paul Eisenbies, Nicole Fettig, Margaret Morris, Amanda Roth, Lori Strong, Ann Stroncek, Jerrel Rutlin, and James Kozlowski for their assistance with the imaging studies; Susie Grathwohl for technical help with animal surgery and postoperative monitoring; and Tom Voller and Curtis Carey for ^{64}Cu production. This material is based on work supported by the National Institutes of Health as a Program of Excellence in Nanotechnology (HL080729). The production of ^{64}Cu is supported by the National Cancer Institute (CA86307).

REFERENCES

- World Health Organization. The Top 10 Causes of Death. Available at: <http://www.who.int/mediacentre/factsheets/fs310/en/index.html>. Accessed November 13, 2009.

- Ibanez B, Badimon JJ, Garcia MJ. Diagnosis of atherosclerosis by imaging. *Am J Med.* 2009;122(1, suppl):S15–S25.
- Langer HF, Haubner R, Pichler BJ, Gawaz M. Radionuclide imaging: a molecular key to the atherosclerotic plaque. *J Am Coll Cardiol.* 2008;52:1–12.
- Davies JR, Rudd JH, Weissberg PL. Molecular and metabolic imaging of atherosclerosis. *J Nucl Med.* 2004;45:1898–1907.
- Laurberg JM, Olsen AK, Hansen SB, et al. Imaging of vulnerable atherosclerotic plaques with FDG-microPET: no FDG accumulation. *Atherosclerosis.* 2007;192:275–282.
- Beer AJ, Schwaiger M. Imaging of integrin $\alpha_v\beta_3$ expression. *Cancer Metastasis Rev.* 2008;27:631–644.
- Jaffer FA, Libby P, Weissleder R. Molecular and cellular imaging of atherosclerosis: emerging applications. *J Am Coll Cardiol.* 2006;47:1328–1338.
- Daniels LB, Maisel AS. Natriuretic peptides. *J Am Coll Cardiol.* 2007;50:2357–2368.
- Ahluwalia A, Hobbs AJ. Endothelium-derived C-type natriuretic peptide: more than just a hyperpolarizing factor. *Trends Pharmacol Sci.* 2005;26:162–167.
- Maack T. The broad homeostatic role of natriuretic peptides. *Arq Bras Endocrinol Metabol.* 2006;50:198–207.
- Maack T. Receptors of atrial natriuretic factor. *Annu Rev Physiol.* 1992;54:11–27.
- Casco VH, Veinot JP, Kuroski de Bold ML, Masters RG, Stevenson MM, de Bold AJ. Natriuretic peptide system gene expression in human coronary arteries. *J Histochem Cytochem.* 2002;50:799–809.
- Naruko T, Ueda M, van der Wal AC, et al. C-type natriuretic peptide in human coronary atherosclerotic lesions. *Circulation.* 1996;94:3103–3108.
- Brown J, Chen Q, Hong G. An autocrine system for C-type natriuretic peptide within rat carotid neointima during arterial repair. *Am J Physiol.* 1997;272:H2919–H2931.
- Leidenfrost JE, Khan MF, Boc KP, et al. A model of primary atherosclerosis and post-angioplasty restenosis in mice. *Am J Pathol.* 2003;163:773–778.
- Maack T, Suzuki M, Almeida FA, et al. Physiological role of silent receptors of atrial natriuretic factor. *Science.* 1987;238:675–678.
- Zheng J, Ochoa E, Misselwitz B, et al. Targeted contrast agent helps to monitor advanced plaque during progression: a magnetic resonance imaging study in rabbits. *Invest Radiol.* 2008;43:49–55.
- Rossin R, Muro S, Welch MJ, Muzykantov VR, Schuster DP. In vivo imaging of ^{64}Cu -labeled polymer nanoparticles targeted to the lung endothelium. *J Nucl Med.* 2008;49:103–111.
- McCarthy DW, Shefer RE, Klinkowstein RE, et al. Efficient production of high specific activity ^{64}Cu using a biomedical cyclotron. *Nucl Med Biol.* 1997;24:35–43.
- Sarembock IJ, LaVeau PJ, Sigal SL, et al. Influence of inflation pressure and balloon size on the development of intimal hyperplasia after balloon angioplasty: a study in the atherosclerotic rabbit. *Circulation.* 1989;80:1029–1040.
- Meding J, Urich M, Licha K, et al. Magnetic resonance imaging of atherosclerosis by targeting extracellular matrix deposition with gadofluorine M. *Contrast Media Mol Imaging.* 2007;2:120–129.
- Sun X, Fang H, Li X, Rossin R, Welch MJ, Taylor JS. MicroPET imaging of MCF-7 tumors in mice via unr mRNA-targeted peptide nucleic acids. *Bioconjug Chem.* 2005;16:294–305.
- Bell MR, Gersh BJ. Restenosis: a clinician's perspective. In: Schwartz RS, ed. *Coronary Restenosis*. Oxford, England: Blackwell Scientific Publications; 1993:15–54.
- Hardoff R, Braegelmann F, Zanzonico P, et al. External imaging of atherosclerosis in rabbits using an ^{123}I -labeled synthetic peptide fragment. *J Clin Pharmacol.* 1993;33:1039–1047.
- Lees AM, Lees RS, Schoen FJ, et al. Imaging human atherosclerosis with ^{99m}Tc -labeled low density lipoproteins. *Arteriosclerosis.* 1988;8:461–470.
- Rudd JH, Myers KS, Bansilal S, et al. Atherosclerosis inflammation imaging with ^{18}F -FDG PET: carotid, iliac, and femoral uptake reproducibility, quantification methods, and recommendations. *J Nucl Med.* 2008;49:871–878.
- Rosen JM, Butler SP, Meinken GE, et al. Indium-111-labeled LDL: a potential agent for imaging atherosclerotic disease and lipoprotein biodistribution. *J Nucl Med.* 1990;31:343–350.
- Worthley SG, Zhang ZY, Machac J, et al. In vivo non-invasive serial monitoring of FDG-PET progression and regression in a rabbit model of atherosclerosis. *Int J Cardiovasc Imaging.* 2009;25:251–257.
- Kologdie FD, Petrov A, Virmani R, et al. Targeting of apoptotic macrophages and experimental atheroma with radiolabeled annexin V: a technique with potential for noninvasive imaging of vulnerable plaque. *Circulation.* 2003;108:3134–3139.
- Ishino S, Mukai T, Kuge Y, et al. Targeting of lectinlike oxidized low-density lipoprotein receptor 1 (LOX-1) with ^{99m}Tc -labeled anti-LOX-1 antibody: potential agent for imaging of vulnerable plaque. *J Nucl Med.* 2008;49:1677–1685.
- Ohtsuki K, Hayase M, Akashi K, Kapiwoda S, Strauss HW. Detection of monocyte chemoattractant protein-1 receptor expression in experimental atherosclerotic lesions: an autoradiographic study. *Circulation.* 2001;104:203–208.